International Journal of Automotive Technology, Vol. 2, No. 3, pp. 93–101 (2001)

Copyright © 2001 KSAE
1229–9138/2001/005–02

ANALYSIS OF IN-CYLINDER FUEL–AIR MIXTURE DISTRIBUTION IN A HEAVY DUTY CNG ENGINE

SEOK Y. LEE[1], KANG Y. HUH[1]*, Y. M. KIM[2] and J. H. LEE[2]

[1]Mechanical Engineering Department, Pohang University of Science and Technology
[2]Engine R&D Group, Korea Institute of Machinery and Materials

(Received 17 February 2001)

ABSTRACT–Distribution of fuel-air mixture has a strong influence on performance and emissions of a compressed natural gas (CNG) engine. In this paper, parametric study is performed by KIVA-3V to investigate fuel-air mixture with respect to injection timing, cycle equivalence ratio and engine speed. With open-valve injection intensive mixing during intake and compression stroke results in relatively homogeneous mixture in the cylinder. Sequential induction of fuel-air mixture and fresh air results in stratification in the cylinder among the test cases at closed-valve injection. There is close similarity in the calculated distributions of the mixture in the cylinder with different cycle equivalence ratios and engine speeds. The results are compared against pressure traces and flame images obtained in a single cylinder engine converted from a 11L six-cylinder heavy duty diesel engine.

KEY WORDS : CNG engine, Injection timing, Engine speed, Equivalence ratio

NOMENCLATURE

ϕ_l : local equivalence ratio
ϕ_m : mean equivalence ratio
ϕ_c : cycle equivalence ratio
σ : standard deviation
γ : specific heat ratio
P_e : nozzle exit pressure
T_e : nozzle exit temperature
ρ_e : nozzle exit density
V_l : volume of a computational cell
P_0 : stagnation pressure
T_0 : stagnation temperature

1. INTRODUCTION

Due to atmospheric pollution and limited oil reserve many fuels such as natural gas, LPG, hydrogen, alcohol, etc. have been considered as promising alternatives for urban transportation. Among them natural gas has a few advantages over other fuels for its lower cost, knocking resistance, and lower level of harmful emissions. Since natural gas has a higher octane number than gasoline, the compression ratio can be raised (Ishii, 1999) to achieve a higher efficiency with a lower rate of fuel consumption. Natural gas engines, however, have lower power and torque than gasoline engines due to lower volumetric efficiency and delayed ignition timing.

There have been recent efforts to overcome these shortcomings of a natural gas engine. Clark *et al.* (1998) reported very low levels of CO and NOx from natural gas vehicles through long term comparison with heavy duty fleet emissions. Hiltner *et al.* (1996, 1997) investigated the impact of the injection timing on in-cylinder fuel distribution in a natural gas engine. They showed in their experimental results that the best injection timing was 60 deg. ATDC in the intake stroke. Arcoumanis *et al.* (1997) investigated the combustion characteristics of gasoline and CNG engines using flame images, pressure traces and exhaust emissions from a single cylinder optical engine. It was shown that the fuel injection timing had significant effects on flame propagation and engine performances such as cyclic variation, IMEP and exhaust emissions.

Of crucial importance for natural gas powered engines is homogeneity of in-cylinder fuel-air mixture at the spark timing. The fuel-air mixture from liquid fuel is largely dependent on atomization and evaporation of the injected fuel droplets, while gaseous injection does not involve the complex phenomena. Mixing of gaseous fuel with ambient air is usually slower than that of liquid fuel due to the lower mass and momentum (Abraham *et al.*, 1994). The mixture formation process in a CNG engine is influenced by several factors such as fuel composition

*Corresponding author. e-mail: huh@postech.ac.kr

(Matthews *et al.*, 1996; Lee *et al.*, 1999; Lee *et al.*, 2000), chamber shape (Miura *et al.*, 2000), injection timing (Hiltner *et al.*, 1996, 1997; Arcoumanis *et al.*, 1997), ignition timing (Arcoumanis *et al.*, 1997), compression ratio (Takagaki *et al.*, 1997), etc. In this paper distribution of fuel-air mixture in the cylinder is numerically predicted with various injection timings, cycle equivalence ratios and engine speeds. The predicted results are evaluated against the experimental observations in a single cylinder optical engine converted from a 11L six cylinder diesel engine.

2. COMPUTATIONAL PROCEDURES

Computations are performed by KIVA-3V (Amsden, 1997), a CFD code for transient, three-dimensional, chemically reactive fluid flows with sprays. The code solves the mass, momentum and energy conservation equations by a combination of explicit and implicit methods on a staggered grid. It has the capability to calculate intake flow with a moving valve model, which is an extension of the snapper algorithm for a piston in KIVA-3 (Amsden, 1993). Valves move with the same velocity according to the given lift profile in KIVA-3V. Valves are closed when the specified minimum valve lift, usually 0.20-0.50 mm, is reached. The boundary conditions around valves are changed with valve closure to avoid excessively small cells.

The computational grid is generated by the commercial software, ICEM CFD/CAE (1993). It is an integrated tool that combines geometry acquisition or creation with grid generation capability. The computational domain consists of a combustion chamber, a piston bowl, an intake valve and a helical intake port to create strong swirl motion during an intake stroke. The valve region involves finer discretization, while the curved profiles are exactly maintained with vertical valve motion. The initial grid is generated with the valve and the piston at their bottom dead center (BDC) positions. The maximum and minimum valve lifts are 13.25 mm and 0.5 mm respectively. Figure 1 shows the grid with about 100,000 computational cells.

Calculations starts at the top dead center (TDC) just after the intake valve opening (IVO). The whole domain is assumed to be initially quiescent at the atmospheric pressure. The boundary condition at the intake port entrance is specified as one atmospheric pressure.

For the given values of P_0 and T_0, the exit condition from the fuel nozzle is estimated by assuming choking in an isentropic process. The conditions known for the gas injector are the stagnation pressure and temperature, P_0 and T_0, and the measured mass flow rate. The properties at the nozzle exit are given as

$$p_e=P_0\left(\frac{2}{\gamma+1}\right)^{\frac{\gamma}{\gamma-1}}=0.385\ \text{MPa} \tag{1}$$

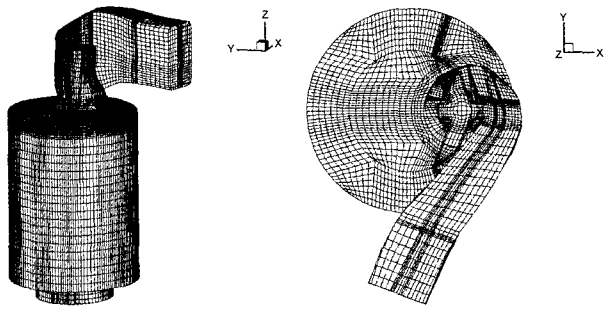

(a) perspective (b) top

Figure 1. Computational grid.

$$T_e=T_0\left(\frac{2}{\gamma+1}\right)=253.20\text{K} \tag{2}$$

$$\rho_e=\rho_0\left(\frac{2}{\gamma+1}\right)^{\frac{1}{\gamma-1}}=3.283\text{kg/m}^3 \tag{3}$$

where the specific heat ratio, γ, is 1.28. The injection conditions are listed in Table 1. The governing conservation equations of mass, momentum, and energy are solved in conjunction with the κ–ε turbulence equations in a compressible form, the fuel mass fraction equation, and the ideal gas equation of state. The run time for each case is typically about 23 CPU hours on Cray C90.

3. ENGINE SPECIFICATIONS

A diagram for the fuel supply system is shown in Figure 2. The high pressure from the fuel tank is reduced to 0.69 MPa by a pressure regulator before the injector. The fuel injector was designed to supply sufficient fuel flow by a driving pressure pulse. The pressure regulator is heated by hot water to prevent the fuel system from freezing due to gas expansion. The air/fuel ratio is controlled by an electronic control system, which also controls fuel meter-

Table 1. Fuel injection conditions.

	Reference case	Parametric study
Equivalence ratio, ϕ	0.667	1.0
Injection timing (CA BTDC)	60	0
Engine speed (rpm)	600	900, 1200
Mass flow rate (kg/s)	3.912	
Injection duration (ms)	15.242	
Injection pressure (MPa)	0.7	
Nozzle diameter (mm)	3.6	
Fuel temperature (K)	288.65	
Fuel density (kg/m^3)	5.242	

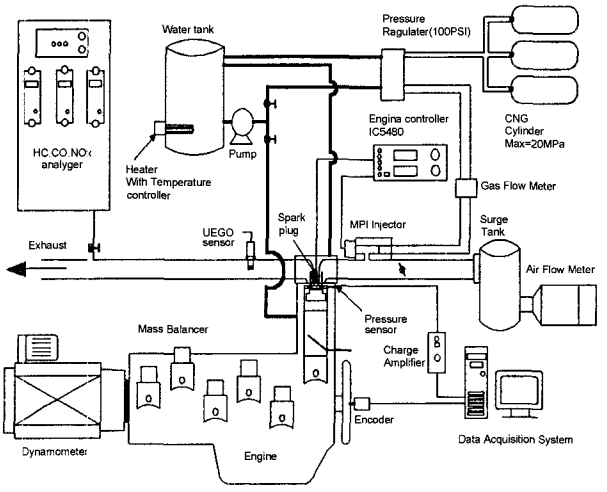

Figure 2. Schematic diagram of the experimental facilities.

Table 2. Engine operating conditions.

Bore (mm)	123
Stroke (mm)	155
Compression ratio	11.8
IVO/IVC (CA)	18 deg. BTDC/34 deg. ABDC

Table 3. CNG composition.

Component	CH_4	C_2H_6	C_3H_8	C_4H_{10}	C_5H_{12}	N_2
Mass fraction	0.800	0.127	0.049	0.022	0.001	0.001

ing, spark timing and injection timing.

The engine operating conditions and the CNG composition are listed in Table 2 and Table 3 respectively. The diagram in Figure 3 shows the start of injection (SOI) timing and the intake valve opening (IVO) and closing (IVC) timings.

The equivalence ratio is defined as the ratio of the actual fuel/air ratio to the stoichiometric fuel/air ratio (Heywood, 1988). In this paper three kinds of equivalence ratios, which are local, mean, cycle equivalence ratios, are introduced. The local equivalence ratio, ϕ_i, represents the mixture composition in the i-th computational cell. Distributions of the in-cylinder mixture composition are investigated on the two cutting planes, AA and BB, in Figure 4. The mean equivalence ratio, ϕ_m, which varies with the crank angle, is the spatially averaged equivalence ratio in the cylinder. The cycle equivalence ratio, ϕ_c, is a constant equivalence ratio averaged over many cycles. The mean equivalence ratio, ϕ_m, is given as

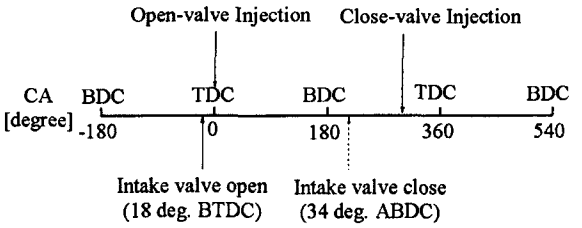

Figure 3. Timing diagram.

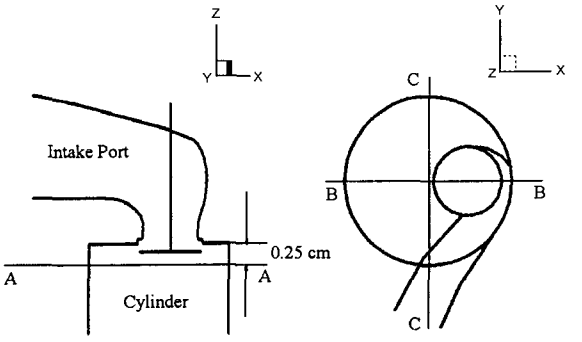

Figure 4. Location of three cutting planes.

$$\phi_m = \frac{\sum_{i=1}^{N} \phi_i V_i}{\sum_{i=1}^{N} V_i} \tag{4}$$

The standard deviation is a statistical term that measures how widely values are dispersed from the average (Press *et al.*, 1992). It is used in this study to provide the degree of inhomogeneity of mixture distribution in the cylinder. The volume-averaged standard deviation is given as

$$\sigma = \sqrt{\frac{\sum_{i=1}^{N} (\phi_i - \phi_m)^2 V_i}{\sum_{i=1}^{N} V_i}} \tag{5}$$

The test cases in the parametric study are listed in Table 1. The reference condition has the closed-valve injection timing of 60 deg. BTDC, the cycle equivalence ratio of 0.667 and the engine speed of 600 rpm. The effects of the injection timing are investigated with respect to the reference condition with the open-valve injection timing of 0 deg. ATDC. The effects of the cycle equivalence ratio and the engine speed are investigated with the stoichiometric ϕ_c and the engine speeds of 900 and 1200 rpm.

4. RESULTS AND DISCUSSION

Since no direct validation against the measurement data is performed in this paper, the following results here may be considered more for qualitative overall trends than for any specific quantitative prediction.

As described in the section 2, the fuel distribution results are based on isentropic choke flow for high pressure, supersonic, transient injection. A uniform velocity profile is specified for fully developed turbulent flow at the nozzle exit. The inflow boundary condition from the measured mass flow rate is employed with the inflow states for CNG gas as determined in the section 2.

4.1. Effects of the Injection Timing

Calculations are carried out for the two injection timings, open-valve injection of 0 deg. BTDC SOI and closed-valve injection of 60 deg. BTDC SOI, both at 600 rpm and ϕ_c. Figure 5 shows variation of the mean equivalence ratio with respect to the crank angle for all test cases. The mean equivalence ratio is slightly overpredicted by about 1% at the end of the compression stroke. Figure 6 shows the standard deviation of the local equivalence ratio for the two different injection timings. It is shown that open-valve injection results in more homogeneous distribution at the ignition timing in the cylinder than closed-valve injection.

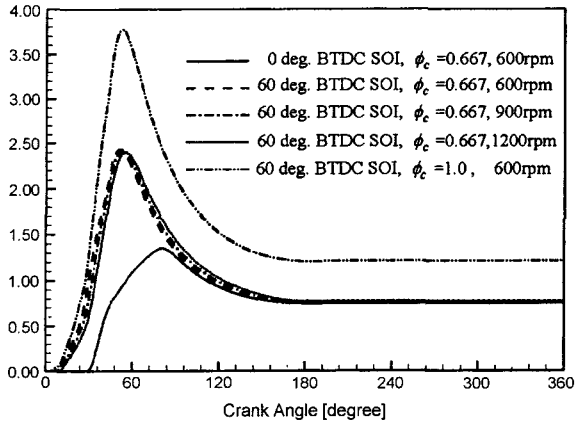

Figure 5. Variation of the mean equivalence ratio in the cylinder.

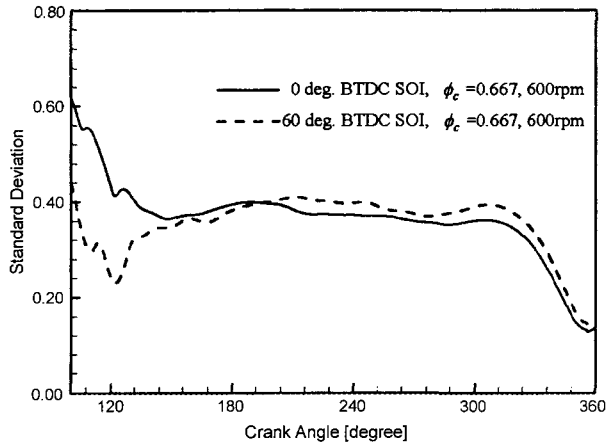

Figure 6. Standard deviation of the local equivalence ratio with different injection timings.

Figure 7 shows distribution of fuel-air mixture on the vertical cutting plane, BB, with open-valve injection of 0 deg. ATDC SOI. Fuel injected mixes with air in the intake port and is drawn into the cylinder during the intake stroke. The intake jet flow carries fuel into the piston bowl at 60 deg. ATDC. By 120 deg. ATDC fuel-air mixture completely fills the cylinder and then only fresh air enters the cylinder until the intake valve closure at 180 deg. ATDC. Mixing is facilitated by tumble motion during the intake stroke, while swirl motion dominates during the compression stroke. Mixing of fuel and air continues to form uniform mixture in the cylinder by 300 deg. ATDC.

Closed-valve injection of 60 deg. BTDC SOI has a different pattern of mixing. Rich mixture forms in the intake port during the period that the intake valve is closed. Figure 8 shows the mixing process in the cylinder during the intake and compression strokes. As the valve opens, the rich mixture in the intake port flows into the cylinder. The cylinder is completely filled with fuel-air mixture by 60 deg. ATDC. At 180 deg. ATDC stratification is observed between rich mixture and fresh air in the cylinder. The stratified distribution remains at 300 deg. ATDC in contrast with open-valve injection. At the ignition timing of 330 deg. ATDC lean mixture exists around the spark plug, while rich mixture exists in the piston bowl. This inhomogeneity may lead to poor combustion quality and large cyclic variation and emissions. The distributions on the horizontal plane through the spark plug location, AA, are presented for the two injection timings in Figure 9. Initial flame from the spark plug may preferentially propagate faster through this rich mixture toward the intake valve.

Combustion characteristics were experimentally investigated by direct imaging of propagating flames and the cylinder pressure. The ignition timing was fixed at 30 deg. BTDC for all cases. Figure 10 shows the sequential images of flame propagation for the two injection timings. The open-valve injection shows more rapid flame propagation than the closed-valve injection. The flame initially propagates toward the intake valve as expected in the calculation results of Figure 9. Figure 11 and 12 show the calculated heat release rates and cylinder pressure traces for the two injection timings. Note that the

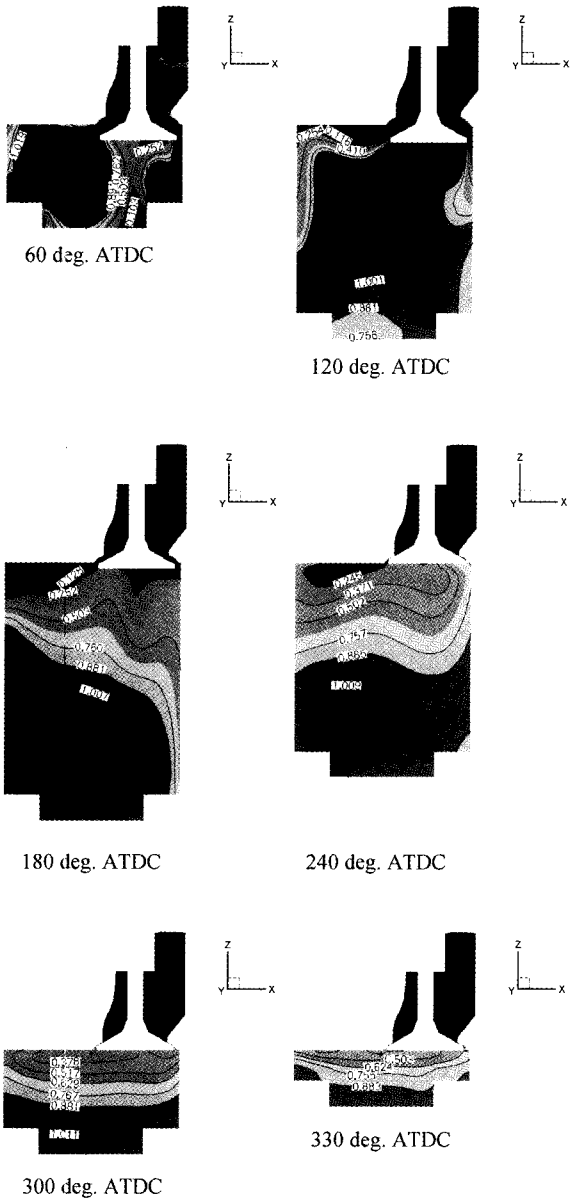

Figure 7. Distribution of the local equivalence ratio on the vertical cutting plane, BB (0 deg. BTDC SOI, ϕ_c=0.667, 600 rpm).

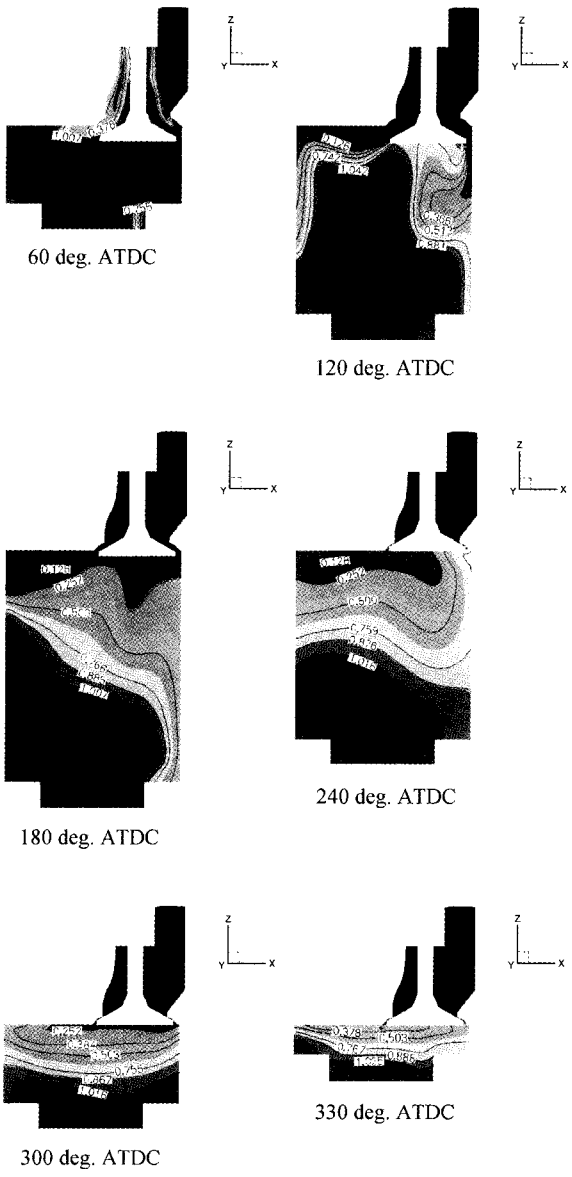

Figure 8. Distribution of the local equivalence ratio on the vertical cutting plane, BB (60 deg. BTDC SOI, ϕ_c=0.667, 600 rpm).

heat release rate with open-valve injection rises more quickly resulting in a higher peak pressure.

4.2. Effects of the Cycle Equivalence Ratio

Calculation is performed for the two cycle equivalence ratios of 0.667 and 1.0 at the speed of 600 rpm and with closed-valve injection. It is to investigate the mixture distribution in the cylinder with different amounts of injected fuel. Close similarity is observed between the two distributions with different cycle equivalence ratios. The standard deviations of the local equivalence ratio in Figure 13 are proportional to the cycle equivalence ratios. The mixture distributions on the horizontal and vertical planes, AA and BB, are shown at the ignition timing in Figure 14. It is obvious that the mixture of the stoichiometric ϕ_c will have lower cyclic variation and faster flame propagation. The images in Figure 15 show that the flame propagation with the stoichiometric ϕ_c is about twice as fast as that with the lean ϕ_c. In Figure 16

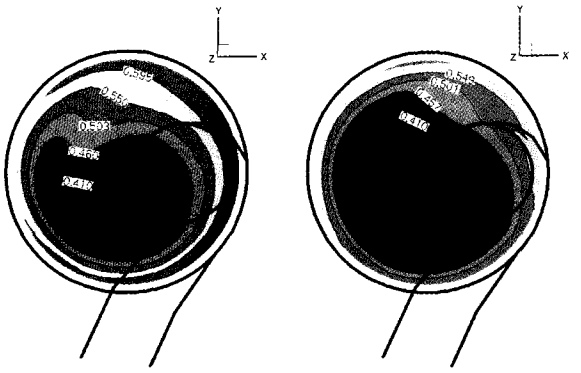

(a) Open-valve injection (0 deg. BTDC SOI)

(b) Closed-valve injection (60 deg. BTDC SOI)

Figure 9. Distribution of the local equivalence ratio on the horizontal cutting plane, AA (ϕ_c=0.667, 600 rpm).

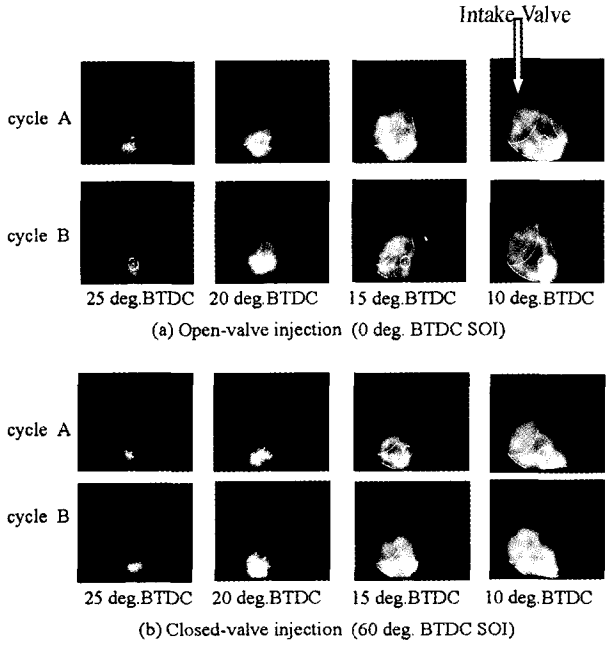

Figure 10. Visualization images of flame propagation for two independent cycles with different injection timings (30 deg. BTDC IGT, ϕ_c=0.667, 600 rpm).

cyclic variations are shown in terms of the images at the crank angles with similar flame areas. These results confirm good qualitative agreement between predicted results and experimental investigations for the two different cycle equivalence ratios.

4.3. Effects of the Engine Speed

The effects of the engine speed are investigated in terms of the mixture distributions at 600, 900, and 1200 rpm. The standard deviations of the local equivalence ratio are

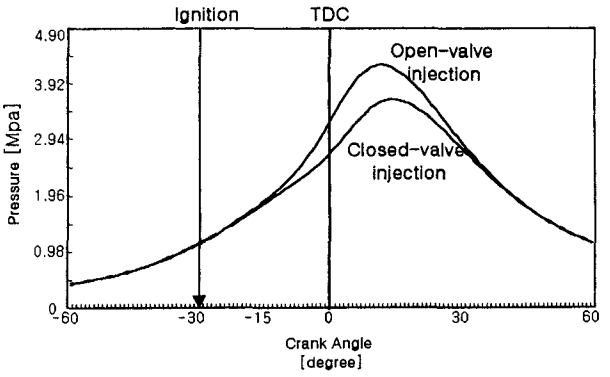

Figure 11. Cylinder pressure trace with different injection timings (30 deg. BTDC IGT, ϕ_c=0.667, 600 rpm).

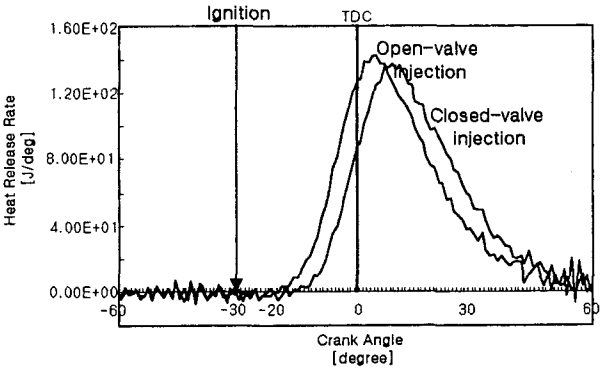

Figure 12. Heat release rate curves with different injection timings (30 deg. BTDC IGT, ϕ_c=0.667, 600 rpm).

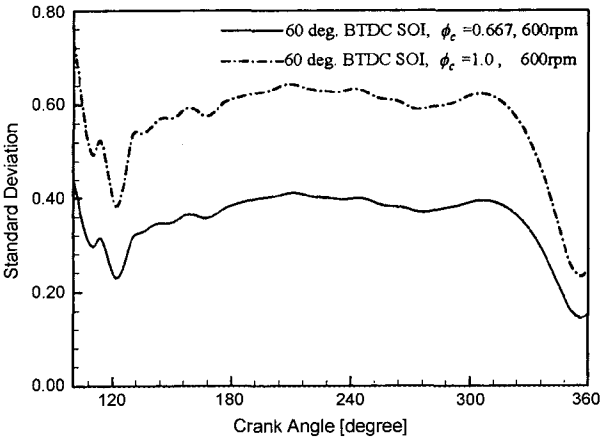

Figure 13. Standard deviation of the local equivalence ratio with different equivalence ratios.

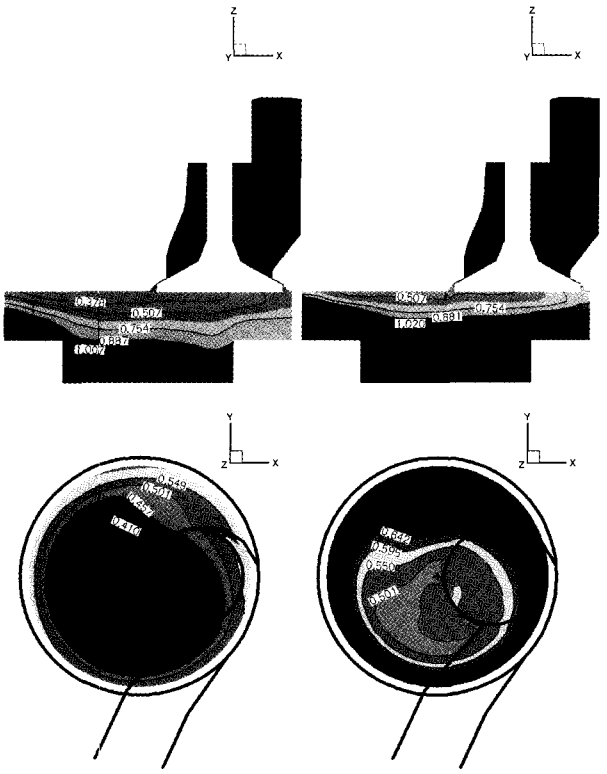

(a) ϕ_c=0.667 (b) ϕ_c=1.0

Figure 14. Distribution of the local equivalence ratio at different engine speeds on the vertical cutting plane, BB, and the horizontal plane, AA (60 deg. BTDC SOI, ϕ_c=0.667).

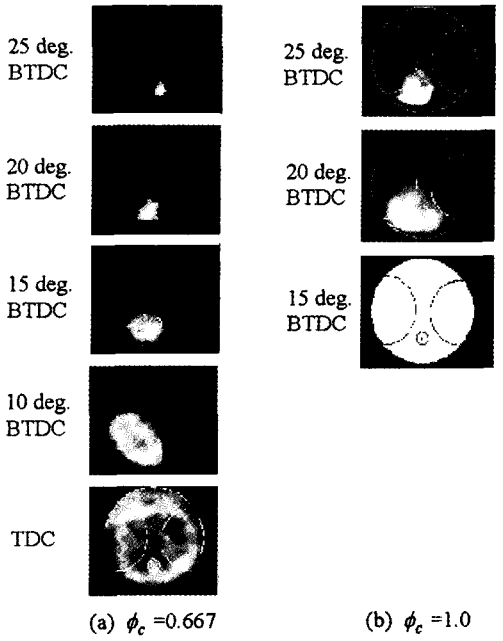

(a) ϕ_c =0.667 (b) ϕ_c =1.0

Figure 15. Visualization images of flame propagation with different mean equivalence ratio (30 deg. BTDC IGT, 600 rpm).

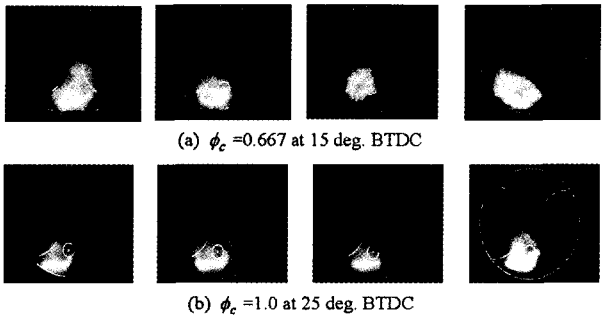

(a) ϕ_c =0.667 at 15 deg. BTDC

(b) ϕ_c =1.0 at 25 deg. BTDC

Figure 16. Cyclic variation in the combustion process with different mean equivalence ratios (30 deg. BTDC IGT, 600 rpm).

shown in Figure 17. The mixture distributions on the horizontal and vertical planes, AA and BB, are shown at the ignition timing in Figure 18. The close similarity in the spatial distributions shows that the turbulent mixing process is scaled by the engine speed. Enhanced mixing by higher turbulent intensity is balanced by the faster time scale with a higher engine speed.

The flame images in Figure 19 show faster propagation of initial flames at a higher engine speed. However, after 15 deg. ATDC the flames at 600 rpm show faster propagation with respect to the crank angle than those at a higher engine speed, 900 rpm. It is due to the dominant influence of a shorter absolute time scale per one degree crank angle at a higher engine speed.

5. CONCLUSION

The fuel-air mixture distributions are calculated to investigate the effects of injection timing, cycle equivalence ratio and engine speed in a CNG engine. The predicted results are compared qualitatively against pressure traces and flame images obtained in the single cylinder test engine. The conclusions of this study are summarized as follows:

(1) With open-valve injection intensive mixing occurs during the intake and compression strokes to result in relatively homogeneous mixture at the ignition timing. With closed-valve injection, on the other hand, rich mixture in the port is first drawn into the cylinder and subsequently fresh air follows. Mixing during the compression stroke is not enough to produce homogeneous mixture in the cylinder. Measured pressure traces and

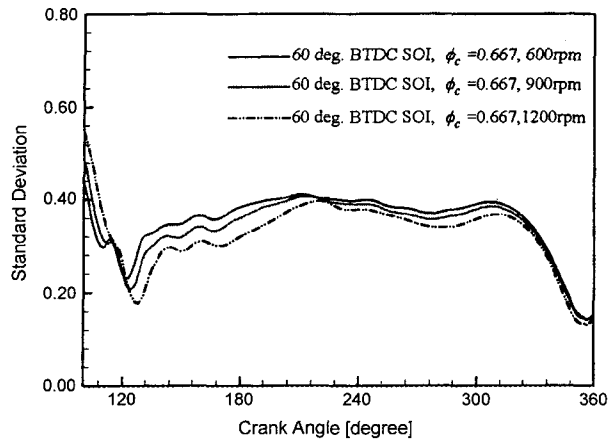

Figure 17. Standard deviation of the local equivalence ratio at different engine speeds.

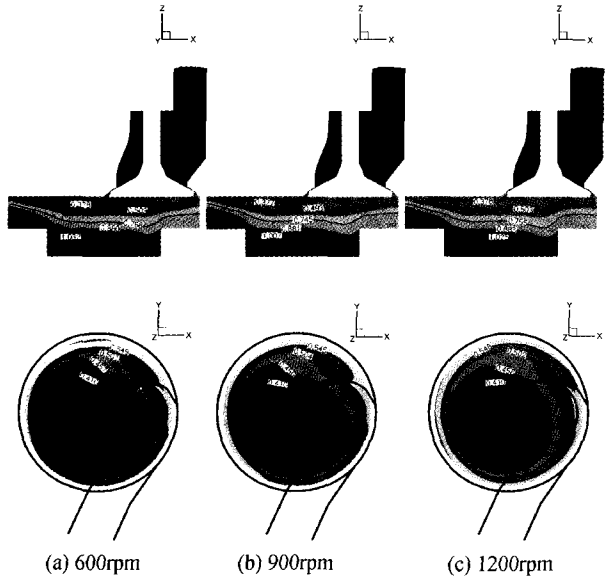

Figure 18. Distribution of the local equivalence ratio at different engine speeds on the vertical cutting plane, BB, and the horizontal cutting plane, AA (60 deg. BTDC SOI, ϕ_c=0.667).

flame images also showed a higher cylinder pressure, faster flame propagation and a shorter combustion duration with open valve injection than with closed valve injection.

(2) The different cycle equivalence ratios, ϕ=0.667 and ϕ=1.0, show close similarity in the mixture distribution of the cylinder. The calculated standard deviation of the local equivalence ratio turns out to be approximately proportional to the injected amount of fuel or the cycle

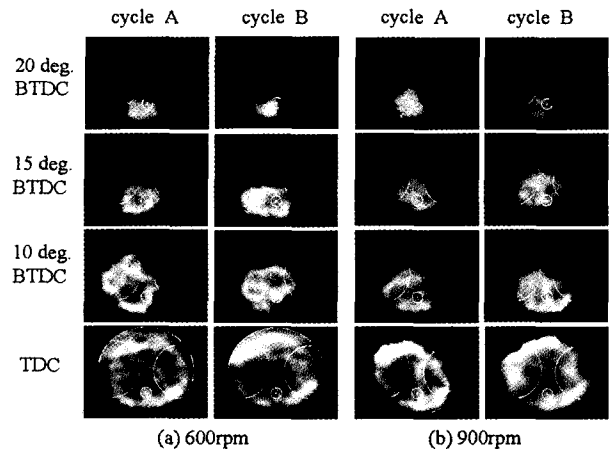

Figure 19. Visualization images of flame propagation at different engine speeds (30 deg. BTDC IGT, ϕ_c=0.667).

equivalence ratio. The higher jet turbulence with the higher cycle equivalence ratio does not seem to have any noticeable effect on the final calculated mixture distribution in the cylinder. The case of the higher cycle equivalence ratio resulted in lower cyclic variations and faster flame propagation in the experiment.

(3) The different engine speeds, 600, 900 and 1200 rpm, also show close similarity in the mixture distribution of the cylinder. It means that the turbulent mixing process is scaled by the mean piston speed or the engine speed for the same engine. Enhanced mixing by higher turbulent intensity is balanced by the faster time scale at a higher engine speed. Initial flame propagation was faster at a higher rpm according to the flame images in the experiment. After the initial period the absolute combustion time had more influence than enhanced mixing by turbulence to result in slower flame propagation at a higher rpm.

ACKNOWLEDGEMENT–The present study has been performed under the Supercomputing Application Support Program of Korea Research & Development Information Center (KORDIC).

REFERENCES

Abraham, J., Magi, V., MacInnes, J. and Bracco, F. V. (1994). Gas versus spray injection: Which mixes faster?, *SAE 940895*. Amsden.

Amsden, A. A. (1993). *KIVA-3: A KIVA Program with Block-Structured Mesh for Complex Geometries*, Los Alamos National Laboratory Report, LA-12503-MS.

Amsden, A. A. (1997). *KIVA-3V: A Block-Structured KIVA Program for Engines with Vertical or Canted Valves*, Los Alamos National Laboratory Report, LA-

13313-MS.

Arcoumanis, C., Bodwin, S. N. and Kim, J. W. (1997). *Analysis of Combustion and Emissions in a Spark-Ignition Engine Fueled by Compressed Natural Gas-Comparison to Gasoline*, Imperial College of Science and Technology, Thermofluids Section Internal Report.

Clark, N. N., Rapp, B. L., Gautum, M. and Wang, W. (1998). A long term field emissions study of natural gas fueled refuse haulers in New York, *SAE 982456.*

Heywood, J. B. (1988). *Internal Combustion Engine Fundamentals*, Mc-Graw Hill Book Company.

Hiltner, J. and Samimy, M. (1996). A study of in-cylinder mixing in a natural gas powered engine by planar laser-induced fluorcence, *SAE 961102.*

Hiltner, J. and Samimy, M. (1997). The impact of injection timing on in-cylinder fuel distribution in a natural gas powered engine, *SAE 971708.*

ICEM CFD: Structured Grid Generation Training. ICEM CFD Engineering.

ICEM CFD/CAE Users Manual (1993). ICEM systems.

ISHII, M. (1999). Research on Lean Combustion Characteristics of Natural Gas Engines, *Proceedings of The 15th Internal Combustion Engine Symposium (International),* Seoul, Korea, 9936030.

Lee, J. S., You, H. S., Han, J. O. and Pang, H. S. (1999). Effects of Natural Gas Composition on Combustion Characteristics in a Gas Fueled Engine, *Proceedings of The 15th Internal Combustion Engine Symposium (International) in* Seoul, Korea, 9936409.

Lee, Y. J. and Kim, G. C. (2000). Effect of Gas Composition on NGV Performance, *Seoul 2000 FISITA World Automotive Congress*, F2000A174.

Matthews, R., Chiu, J. and Hilden, D. (1996). CNG composition in Texas and the effects of composition on emissions, fuel economy, and driveability of NGVs, *SAE 962097.*

Miura, A., Honjou, F. and Nakamura, A. (2000). Further Development of Fuel Consumption for Heavy-Duty CNG Engine, *Seoul 2000 FISITA World Automotive Congress*, F2000A173.

Press, W. H., Teukolsky, S. A., Vetterling, W. T. and Flammery, B. P. (1992) *Numerical Recipes in C: The Art of Scientific Computing*, Press, W. H..

Takagaki, S. S. and Raine, R. R. (1997). The effects of compression ratio on nitric oxide and hydrocarbon emissions from a spark-ignition natural gas fueled engine, *SAE 970506.*